Waste Management 141 (2022) 194–201

Contents lists available at ScienceDirect

Waste Management

journal homepage: www.elsevier.com/locate/wasman

Chemical looping gasification using Nickel-containing electroplating sludge and dyeing sludge as oxygen carrier

Jing Han [a,b,c,d,1], Rui Shan [a,b,c,d,1], Jing Gu [a,b,c,d], Haoran Yuan [a,b,c,d,*], Yong Chen [a,b,c]

[a] Guangzhou Institute of Energy Conversion, Chinese Academy of Sciences, Guangzhou 510640, Guangdong, China
[b] Southern Marine Science and Engineering Guangdong Laboratory (Guangzhou), Guangzhou 511458, Guangdong, China
[c] School of Engineering Science, University of Science and Technology of China, Hefei 230027, Anhui, China
[d] CAS Key Laboratory of Renewable Energy, Guangdong Provincial Key Laboratory of New and Renewable Energy Research and Development, Guangzhou 510640, China

ARTICLE INFO

Keywords:
Electroplating sludge
Dyeing sludge
Oxygen carrier
Chemical looping gasification
Waste treatment

ABSTRACT

Nickel-containing electroplating sludge (NiES) and dyeing sludge (DS) were used to prepare oxygen carriers (OCs) for chemical looping gasification (CLG) of DS. X-ray diffraction (XRD), surface area and porosity analysis were employed to investigate the crystal structure and pore structure of NiES and DS ash OCs. It was found that OCs prepared at 850 ℃ for 8 h (850NiES8, 850DS8) exhibited good characteristics in terms of pore structure. X-ray fluorescence (XRF), hydrogen temperature programmed reduction (H_2-TPR) and thermo-gravimetric (TG) were employed to explore the elemental composition, reactivity, redox behavior and their effect on DS pyrolysis of the two selected OCs. The influence of mass ratio of 850NiES8, 850DS8 to DS (850NiES8/DS, 850DS8/DS) and reaction temperature on DS CLG were investigated. It showed that the addition of two OCs significantly promoted the gas yield of DS while accelerating the gasification process. It showed a better performance of 850NiES8 than that of 850DS8 when it was below 900 ℃. On the other side, 850DS8 showed more advantage between 900 and 950 ℃. And high carbon conversion (η_C) of 80.94%,77.59% and acceptable valid gas yield (V_g) of 0.192,0.190 Nm^3/kg could be obtained at 850 ℃ when 850NiES8/DS, 850DS8/DS were 1, respectively. In this process, the reduction and energy recovery of dyeing sludge were implemented, and two promising OCs (850NiES8, 850DS8) were developed. In addition, a new harmless method of NiES recycle treatment was also provided.

1. Introduction

As a novel technology, chemical looping gasification (CLG) provides oxygen for gasification from lattice oxygen in oxygen carrier (OC). CLG has many advantages compared with traditional gasification technology (Wang et al., 2020c; Zhang et al., 2021a, 2021b). It saves the cost of gasification agent, and gains higher syngas calorific value. Besides, OC also acts as a catalyst (Sajjadi et al., 2021; Sampron et al., 2020) which can effectively reduce thermal NO_x yield (Pérez-Astray et al., 2019), in the condition that the fuel is not in direct contact with air and the operating temperature is relatively low.

Excellent OC, which is cheap, has high redox activity, high mechanical strength and anti-sintering ability (Cheng et al., 2021; Yang et al., 2019a) is the key of CLG. OC is generally composed of active components and inert carriers. The active components are usually metal oxides such as Fe, Cu, Ni, Mn, Co and non-metal oxides like $CaSO_4$ (Liu et al., 2019; Wang et al., 2020b). In recent year, ore and waste residues are joined much attention as OC because of their rich metal content, low cost and environmental friendliness (Sarafraz & Christo, 2020; Wang et al., 2021a, 2021b, 2021c; Yang et al., 2021). For example, Zhang et al. (2019) combined natural iron ore with biomass ash to prepare OC for chemical looping combustion (CLC). Similarly, Cuadrat et al. (2012) found that ilmenite could be used as a low cost and promising material for OC in CLC. In another work, Yang et al. (2017) prepared OC from phosphogypsum (PG) for lignite CLG and found $CaSO_4$ was almost converted to CaS over 850 ℃. Di et al. (2018) first explored the use of

* Corresponding author at: Guangzhou Institute of Energy Conversion, Chinese Academy of Sciences, Guangzhou 510640, Guangdong, China.
E-mail address: yuanhr@ms.giec.ac.cn (H. Yuan).
[1] Both authors contributed equally to this work.

https://doi.org/10.1016/j.wasman.2022.01.016
Received 28 October 2021; Received in revised form 6 January 2022; Accepted 13 January 2022
Available online 8 February 2022

steel slag (a typical metallurgical waste) as OC and found the optimized reduction temperature for it was 750 °C.

Electroplating sludge (ES) is a kind of solid waste produced by adding alkaline substances and flocculants (aluminum sulfate, ferric sulfate, ferric chloride, etc.) to metal electroplating and circuit board etching wastewater. With large amount and unstable state, ES is extremely harmful to the environment (Chen et al., 2021). There are about 15,000 electroplating enterprises in China with a production capacity of 300 million m^2 electroplating area. And electroplating wastewater which is about 4 billion m^3 is discharged every year, producing around 10 million tons ES (Zhang et al., 2020a). Traditional treatments of ES mainly include solidification and heat treatment for volume reduction. Resource-based treatments such as roasting leaching, biological recovery of heavy metals and hydrometallurgy have been studied recently. Wang et al. (2018) proposed a centrifuge electrode for high-purity Cu powders recovery by one-step electrodeposition from ES leaching solution. In another work, Tian et al. (2019) proposed a low-carbon redox refining process for valuable metals recovery in ES. The ratios of Pb, Sn, Zn removal reached 90.77%, 95.14%, 99.92% within 60 min, respectively. However, the process of extracting metal from ES is complex and it is difficult to achieve resource recovery. It is known that electroplating wastewater contains a large amount of metal ions (Zhou et al., 2019) .The common flocculants, such as iron sulfate, ferric chloride, are rich in Fe. It is possible to prepare OC from ES, for nickel-containing electroplating sludge (NiES) is rich in Ni element and has the second large production among ES. However, there is no research on preparing OC by NiES so far.

Dyeing sludge (DS) is a kind of residual waste produced from dyeing wastewater treatment. The main components of DS are organic matter, dyes, auxiliaries, heavy metals. With the development of printing and dyeing industry, DS production continues increasing, of which improper treatment may lead to serious environment problem. Higher volatile content than most sludge and lower price than most biomass make DS a promising gasification raw material. However, there is still little research on DS CLG until now. Chen et al. (2016) investigated sludge gasification in fluidized bed using hematite as OC which improved carbon conversion (η_C) to 78.57%. In another work, Deng et al. (2019) investigated sludge gasification carried out in fixed bed using copper slag calcined at 1100 °C as OC, which increased η_C to 70.20% with valid gas yield of 0.23 Nm^3/kg. The reduction and energy recovery of DS still need further study. CLG of DS can be an effective way for its resource utilization. Meanwhile, DS can also prepare OC because of its high metal content like Fe (Ksepko, 2013).

Thus, the object of this work is to find cheap and good-performing OCs for CLG, study harmless NiES recycle treatment and realize the reduction and energy recovery of DS. In this work, NiES and DS were used to prepare low-cost OCs for the first time. The composition, structure, reactivity and cycle stability of the selected OCs were investigated. Then, DS CLG was conducted in a fixed bed reactor, where the effects of mass ratio of OC to DS and reaction temperature were investigated.

2. Experimental section

2.1. Materials

Raw DS collected from Foshan Datang sewage treatment plant was dried in 105 °C oven until the mass was constant and then sieved to 90 mesh. The lower calorific value of DS is 8.52 MJ/kg. The proximate and ultimate analyses are shown in Table 1. Same analyses of other two kinds of sewage sludge (SS) collected from Huizhou (SS1) and Foshan (SS2) sewage treatment plants were also conducted for comparison. It can be seen that DS has higher volatile content and carbon content than that of other two kinds of sludge, which means DS can produce more combustible gas. Therefore, DS is a suitable gasification raw material.

Raw NiES collected from an electroplating plant in Guangzhou was dried in 105 °C oven until the mass was constant and then sieved to 70 mesh. NiES and DS were calcined in a tubular furnace in air atmosphere (250 mL/min) at 700, 850 and 900 °C for 3 h, respectively to obtain OCs 700NiES3, 850NiES3, 900NiES3, 700DS3, 850DS3, 900DS3. NiES and DS were calcined in a tubular furnace in air atmosphere (250 mL/min) at 850 °C for 5 h and 8 h, respectively to obtain OCs 850NiES5, 850NiES8, 850DS5, 850DS8.

Table 1
Proximate and ultimate analysis of three kinds of sludge.

Sludge type	Proximate analysis (wt.%, d)			Ultimate analysis (wt.%, d)		
	V	A	F_C	C	H	N
DS	43.37	54.71	1.92	22.09	3.32	1.68
SS1	32.97	65.56	1.47	15.32	3.06	2.38
SS2	38.12	59.09	2.79	16.56	3.38	2.50

2.2. Material characterization

The crystal structure of NiES, DS and OCs were analyzed by an X-ray diffraction (XRD, X'Pert Pro MPD) using Cu K_α radiation (40 kV, 40 mA), and the diffraction angle (2θ) of the samples was scanned at a scanning rate of 2°/min from 5° to 80°. Pore structures of the samples were measured by N_2 physisorption at −196 °C using a Micromeritics ASAP 2010 instruments. Optimal OC preparation condition was determined after crystal and pore structure analyses.

After that, the elemental composition of NiES, DS and the selected OCs were analyzed by wavelength dispersive X-ray fluorescence spectrometer (XRF, AXIOSmAX-PETRO). Hydrogen-temperature programmed reduction (H_2-TPR, chemstrat) was used to investigate the reactivity of the selected OCs. 0.1 g sample was heated in the adsorption instrument from 30 to 200 °C at 10 °C/min, and then cooled to 50 °C in Ar atmosphere (50 mL/min) to remove moisture in sample. After that the sample was heated to 1000 °C at 10 °C/min in 10% H_2 atmosphere (Ar balance, 50 mL/min). A thermo-gravimetric analyzer (TG, NETSCH STA409C) was used to analyze the redox behaviors of the selected OCs. In the experiment, 10 mg sample was heated from 30 to 850 °C at 10 °C/min in air atmosphere (45 mL/min). In the reduction stage, 5% H_2 (Ar balance, 45 mL/min) was introduced to the reaction system for 30 min. In the oxidation stage, dry air (45 mL/min) was introduced for 15 min. N_2 (55 mL/min) was introduced for 5 min before and after each reduction stage to avoid mixing H_2 and air. 10 redox cycles have been carried out. The effect of the selected OCs on DS pyrolysis was analyzed by rapid heating TG analyzer (NETSCH SDT650). The test samples are DS, OCs, mixture of DS and OCs, mixture of DS and Al_2O_3. 5 mg sample was heated from 30 to 900 °C at the rate of 10 °C/min with high purity N_2 as protective gas (30 mL/min).

2.3. Fixed–bed setup and procedure

CLG experiment of DS was conducted in a fixed bed reactor, and experimental device is shown in Fig. 1. The quartz tube is 800 mm in length, 17 mm in inner diameter and 23 mm in outer diameter. The quartz basket is 50 mm in length, 13 mm in inner diameter and 15 mm in outer diameter, with several holes distributed at the bottom. Before the experiment, the basket was placed at the top of the quartz tube, and 0.5 g quartz cotton was padded at the bottom of the basket. DS and OC were evenly mixed (mass of DS was 0.45 g) and put into basket. During the experiment, the flow rate of N_2 introduced into the reactor was 100 mL/min while device was heated from 30 °C to the reaction temperature, then switched to 20 mL/min. After 5 min of stabilization, the basket was put down to the middle of heating section, and gas collection bag was used to collect gas for 40 min (every 20 min). The gas composition was analyzed by gas chromatograph (Agilent 7890).

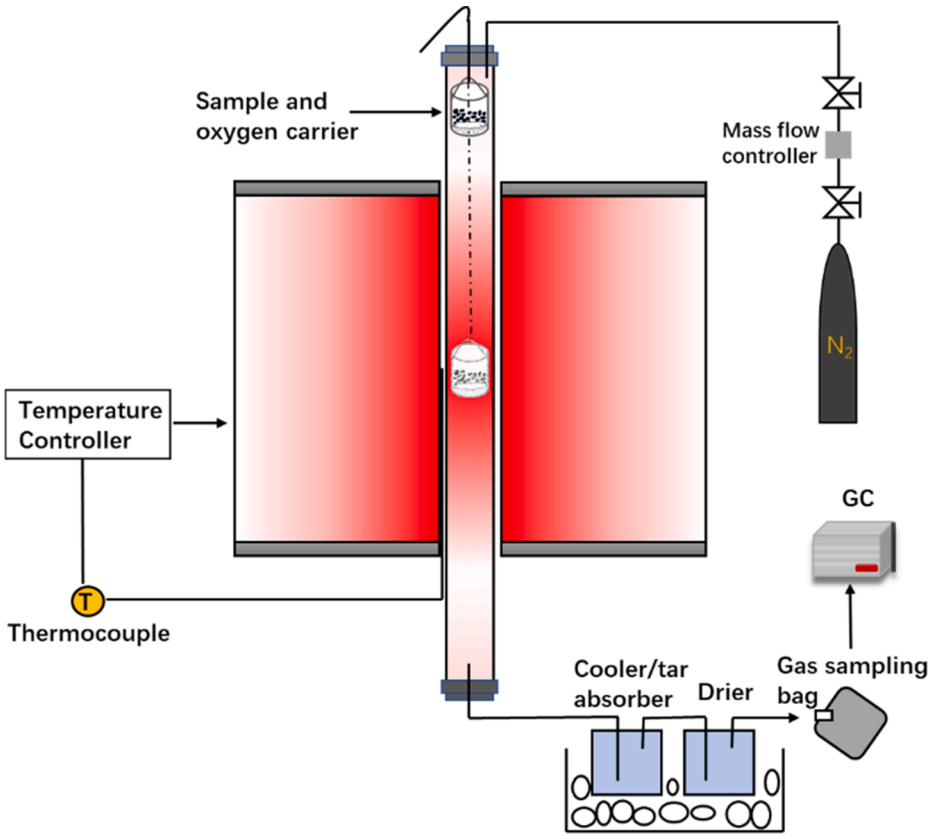

Fig. 1. Schematic diagram of fixed bed reactor.

2.4. Data evaluation

The total volume of outlet gas V_{out} (L) is calculated as Eq. (1). Where q_{N_2} (mL/min) is the volumetric flow of N_2.C_{N_2} (%) is the volume concentration of N_2 collected in the outlet. t_0, t_e (min) are the beginning and ending times of gasification, respectively.

$$V_{out} = \frac{\int_{t_0}^{t_e} q_{N_2} dt}{1000 \times C_{N_2}} \tag{1}$$

The yield of each dry and N_2 free basis gas product (Y_i, Nm^3/kg) yielded from unit mass of DS is calculated as Eq. (2). i represents H_2, CO, CO_2, CH_4, C_2H_2, C_2H_4, C_2H_6, C_3H_6, C_3H_8. C_i (%) represents volume concentration of i collected in the outlet. m_{DS} (g) is the mass of DS.

$$Y_i = \frac{V_{out} \times C_i}{m_{DS}} \tag{2}$$

The carbon conversion η_C (%) is calculated as Eq. (3). C_C (%) represents carbon content of DS. C_2H_m represents C_2H_2, C_2H_4, C_2H_6. C_3H_m represents C_3H_6, C_3H_8.

$$\eta_c = \frac{12 \times V_{out} \times \left(C_{CO} + C_{CO_2} + C_{CH_4} + 2C_{C_2H_m} + 3C_{C_3H_m}\right)}{22.4 m_{DS} C_c} \times 100\% \tag{3}$$

The valid gas yield (V_g, Nm^3/kg) refers to the volume of combustible gas produced from unit mass of DS, and calculated as Eq. (4).

$$V_g = \frac{V_{out} \times \left(C_{H_2} + C_{CO} + C_{CH_4} + C_{C_2H_m} + C_{C_3H_m}\right)}{m_{DS}} \tag{4}$$

The gas yield (G_v, Nm^3/kg) refers to the volume of dry and N_2 free basis gas yielded from unit mass of DS, and calculated as Eq. (5).

$$G_v = V_g + \frac{V_{out} \times C_{CO_2}}{m_{DS}} \tag{5}$$

The oxygen carrying capacity (R_o, %) of OC is calculated as Eq. (6). Where m_{oxi} (g) is the mass of fully oxidized OC before reduction, m_{redu} (g) is the mass of fully reduced OC after reduction.

$$R_O = \frac{m_{oxi} - m_{redu}}{m_{redu}} \tag{6}$$

3. Results and discussions

3.1. Characterization of OCs

3.1.1. XRD analysis

Fig. R1 and R2 (in the Supplementary material) demonstrate the XRD patterns of different NiES and DS ash OCs. As shown in Fig. R1, it cannot identify any phase in raw NiES which indicates that it is amorphous, and most metal species exist in the form of amorphous hydroxide (Peng et al., 2020a; Zhou et al., 2019). This is because NiES is a flocculation precipitation formed by electroplating wastewater's coagulation and destabilization, and it has low crystallinity and no stable crystal structure, which is consistent with the XRD results. As calcination temperature rises, obvious peaks such as Fe_2O_3, NiO, $NiFe_2O_4$, $CaSO_4$ and a small amount of CaO can be observed. The morphologies of 850NiES3, 850NiES5, 850NiES8 and 900NiES3 have no obvious difference when calcination temperature reaches 850 °C, while new peaks of Fe_2O_3 and CaO appear. It shows that the crystallinity of NiES ash increases as calcination temperature rises, which is consistent with the research result of Peng et al. (2020b). After calcination at 850 °C for 3 h, the phase of NiES ash is stabilized. As shown in Fig. R2, raw DS is also in an amorphous state as raw NiES. The peaks of Fe_2O_3 can be seen clearly after calcination. There is no obvious difference between the patterns of

every DS ash OCs.

3.1.2. Pore structure analysis

The pore structures of NiES and DS ash OCs are shown in Table 2. Specific surface area, total pore volume and average pore diameter of the samples decreased gradually as temperature rises under same calcination time. The specific surface areas of NiES and DS ash OCs decreased from 15.73, 1.39 m^2/g at 700 °C to 7.72, 0.51 m^2/g at 900 °C, respectively. When calcination temperature reached 850 °C, the specific surface areas of NiES and DS ash OCs increased from 8.62, 0.87 m^2/g at 3 h to 10.63, 1.34 m^2/g at 8 h, respectively. It is known to us that the main reason affecting OC's performance is the sintering under high temperature working condition, which leads to the densification of OC. The porous structure with large specific surface area is conducive to the full contact between OC and syngas, and also makes OC more efficient in catalyzing tar cracking. Stable crystal structure has not been formed at 700 °C, higher calcination time enhances the mechanical strength of OC but also expends more energy. Therefore, 850 °C and 8 h is the suitable preparation condition. The specific surface areas of 850NiES8 and 850DS8 are higher than most of the OCs that have been studied (850NiES8, especially) (Cao et al., 2021; Wang et al., 2019).

3.1.3. Elemental composition analysis

After calcination, the residues' mass fraction of 850NiES8, 850DS8 are 73.4%, 52.87%, respectively. As shown in Table 3, the mass fraction of metal elements increases significantly. Fe, Ni and Ca basically remained in 850NiES8. While Fe is the main element of 850DS8 and some of it has been lost after calcination. According to XRD patterns, Fe_2O_3, NiO, $NiFe_2O_4$ and a small amount of $CaSO_4$ are the active components of 850NiES8 and Fe_2O_3 is the effective component of 850DS8.

Previous studies have shown that NiO has high reactivity but poor stability with high price (Zheng et al., 2020). $CaSO_4$ which has high oxygen loading but poor reactivity and stability, is easy to obtain. Iron based OC is considered as the most promising OC candidate because it is stable, cheap, non-toxic and environmental friendly (Huang et al., 2016). However, pure iron oxide often loses some oxygen carrying capacity during redox cycles due to its thermal sintering (Ma et al., 2020). Therefore, the preparation of composite OC has always drawn more attentions because the active components can make up for each other's defects and fully utilize. Huang et al. (2019) prepared $NiFe_2O_4$ for chemical looping steam reforming and found it has stronger oxidation performance than Fe_2O_3. Yang et al. (2019b) prepared Fe/phosphogypsum composite OC which had better reactivity and recyclability compared with phosphogypsum. The reactivity of $NiFe_2O_4$ was between NiO and Fe_2O_3, and NiO had no sintering phenomenon which could reduce CLG reaction temperature.

3.1.4. H_2 -TPR analysis

The TPR profiles of 850NiES8 and 850DS8 are shown in Fig. R3. The reduction peak of 850NiES8 is observed around 679 °C, of which there is no obvious side peak. 850NiES8 is completely reduced below 900 °C. Previous studies have shown that the reduction peak of $CaSO_4$ appears near 950 °C (corresponding reaction: $CaSO_4 \rightarrow CaS$), the peaks of Fe_2O_3 appear at about 420 °C, 630 °C, 800 °C (corresponding reaction: $Fe_2O_3 \rightarrow Fe_3O_4$, $Fe_3O_4 \rightarrow FeO$, $FeO \rightarrow Fe$) (Zhang et al., 2020b), and the peak of NiO appears at about 360 °C (corresponding reaction: $NiO \rightarrow Ni$) (Silvester et al., 2016). The oxides are continuously reduced at 400–900 °C which suggests the obviously interaction among $CaSO_4$, Fe_2O_3 and NiO of 850NiES8. Consequently, the above results show that 850NiES8 exhibits satisfactory reaction activity.

As Fig. R3 shows, the main reduction peak of 850DS8 is observed around 780 °C and the two side peaks appear at 628 °C and 856 °C. It is obviously that peaks of 850DS8 are weaker than that of 850NiES8. Since oxidizability of the samples is mirrored by H_2 reduction area, a larger area implies a higher reactivity, and 850NiES8 presents better reactivity than 850DS8.

Table 2
The pore structures of NiES, DS and NiES, DS ash OCs.

Samples	Specific surface area (m^2/g)	Total pore volume (cm^3/g)	Average pore Diameter (nm)
NiES	74.08	0.1266	3.42
700NiES3	15.73	0.0961	12.22
850NiES3	8.62	0.0461	10.70
850NiES5	10.12	0.0480	9.50
850NiES8	10.63	0.0460	17.32
900NiES3	7.72	0.0266	6.89
DS	15.37	0.0611	16.49
700DS3	1.39	0.0045	12.81
850DS3	0.87	0.0039	8.88
850DS5	1.18	0.0048	8.10
850DS8	1.34	0.0045	6.69
900DS3	0.51	0.0022	17.29

Table 3
Elemental composition given in wt. % of NiES, 850NiES8, DS, 850DS8.

Samples	Fe	Ni	Ca	Si	Al	Na	S
NiES	20.20	16.13	5.26	0.52	0.67	–	1.91
850NiES8	27.19	21.64	7.99	0.57	0.73	–	1.99
DS	22.05	–	2.32	2.11	0.50	3.96	7.18
850DS8	39.51	–	3.12	3.05	0.82	7.33	6.06

3.1.5. The redox behaviors of OCs evaluated by TGA

Fig. R4 depicts the weight loss curves of 850NiES8 and 850DS8 during 10 redox cycles. The mass reduction before the first cycle may be due to the evaporation of water in the sample. It can be seen from Fig. R4, the weight variation of 850NiES8 between reduced and oxidized state evidently increases in the second cycle. The average R_o of 850NiES8 is about 18.46% in first 5 cycles, about 17.76% in last 5 cycles and about 18.11% in whole 10 cycles, respectively. Fig. R5 shows that the average R_o of 850DS8 is about 17.15% in first 5 cycles, 15.98% in last 5 cycles and 16.62% in whole 10 cycles, respectively. The redox cycles are stable after 3 cycles and the sintering of 850DS8 is more obvious than 850NiES8.

It can be seen that the two OCs both need an activation process to possess stable redox reactivity. In this activation process, reactions between OC and gas result in many air passages in OC, which makes lattice oxygen develop further and the reduction is carried out more thoroughly as every redox conducted. The specific surface area of OC will slightly increase. This process of 850NiES8 is shorter than 850DS8. The R_o of 850DS8 is a little lower than 850NiES8 in each cycle. The oxidation reaction of two OCs proceeds faster than their reduction reaction. Generally, 850NiES8 and 850DS8 maintain a high R_o which suggests that they can provide sufficient oxygen for gasification. They both have good renewability and cycle stability, while the performance of 850NiES8 is better than 850DS8.

3.1.6. The effect on DS pyrolysis of OCs evaluated by TGA

DS850NiES8, DS850DS8 and $DSAl_2O_3$ were prepared by mixing DS with 850NiES8, 850DS8 and Al_2O_3 at a mass ratio of 1:1. The TG experiment results are shown in Fig. R5. As Fig. R5(a) shown, there is almost no weight loss of 850NiES8 and 850DS8 in N_2 atmosphere, and their TG curves nearly coincide. When temperature reaches 900 °C, the weight losses are 55.07% of DS, 30.66% of $DSAl_2O_3$, 39.29% of DS850NiES8 and 36.91% of DS850DS8. OCs can obviously promote DS's pyrolysis above 635 ℃.

As Fig. R5(b) shows, the conversion of DS is divided into three stages: at the first stage (below 150 °C), the weight loss peak of DS is caused by the evaporation of water in sample; at the second stage (150–500 °C), DS has weight loss peaks at 255 °C and 368 °C, respectively. That may be due to the cracking of volatile matter and the decomposition of lipids

and carbohydrates (Wang et al., 2020a); Specifically, at the third stage (500–900 °C), DS has weight loss peaks at 708 °C and 830 °C, which can be due to the transformation of fixed carbon, decomposition and reaction of inorganic matter in sludge (Lin et al., 2016). The weight loss peaks of DS850NiES8 and DS850DS8 at the third stage are 690 °C, 725 °C and 680 °C, 770 °C, respectively.

All the samples exhibit no obvious difference in the first two stages. But at the third stage, 850NiES8 and 850DS8 significantly promote DS's pyrolysis by releasing lattice oxygen, where the second weight loss peak at this stage of DS850DS8 is obviously weaker than DS850NiES8, which means 850NiES8 can offer more oxygen and exhibits better reactivity than 850DS8. At 900 °C, the mass loss rates of DS850NiES8 and DS850NiES8 are close to 0, which indicates the pyrolysis of DS has been completed, and the residual ash will not be further cracked or reacted. However, the mass loss rates of DS and $DSAl_2O_3$ are still significantly less than 0 at 900 °C, which means the weight loss has not been completed.

3.2. Fixed bed experiments

3.2.1. Effect of oxygen addition

The effect of mass ratio of 850NiES8, 850DS8 to DS (850NiES8/DS, 850DS8/DS) on DS gasification was investigated. The results of 40-min sampling time are shown in Fig. 2. With the increase of 850NiES8/DS from 0 to 3, CH_4 yield fluctuates in a certain range, H_2 decreases gradually, CO reaches its maximum at 850NiES8/DS of 0.5, V_g reaches its maximum (0.223 Nm^3/kg) at 850NiES8/DS of 0.5, and CO_2 yield gradually increases. When 850NiES8/DS increases to 1, η_C and G_v reach their maximum (80.94%, 0.373 Nm^3/kg). When 850DS8 is introduced to the reaction, Y_i basically shows same trend, η_C and G_v reach their maximum (76.37%, 0.354 Nm^3/kg) at 850DS8/DS of 1 while V_g gradually decreases.

On the one hand, OC can provide lattice oxygen so that combustible gas will react with OC to generate CO_2 and H_2O, which explains the downtrend of V_g and the uptrend of CO_2. On the other hand, OC promotes the decomposition of sludge and the secondary cracking of tar (tar → H_2 + CO + C_nH_m). Furthermore, the carbon in sludge can react with OC to generate CO. Thus V_g slightly increases when 850NiES8/DS is added to 0.5, and η_C, G_v significantly increase when 850NiES8/DS and 850DS8/DS are added to 1. η_C and G_v begin to decrease when 850NiES8/DS and 850DS8/DS exceed 1. This may because that excessive addition of OC may hinder the release of volatile matter, block mutual reactions, and slow down heat transfer from fixed bed to sludge. As shown in Fig. 3, the addition of the two OCs both significantly accelerates the gasification of DS. When 850NiES8/DS and 850DS8/DS are 1, the conversion of carbon is basically completed within 20 min, and H_2 in combustible gas is not completely released. Generally, a small amount of OC can significantly promote the conversion of DS and shorten the time required for fully gasification. V_g, η_C, G_v can reach their maximum when 850NiES8/DS is 0.5, 1, and 1, respectively. The addition of 850NiES8 is more conducive to DS gasification than 850DS8.

3.2.2. Effect of reaction temperature

The results of 40-min gas sampling time are presented by Fig. 4 as reaction temperature rises from 750 to 950 °C. Considering the sludge disposal principle of reduction priority, the mass ratio of OC to DS was fixed at 1. When 850NiES8/DS is 1, η_C gradually increases from 71.95% to 84.53%. H_2 and CO yield gradually increase, CO_2 yield reaches its maximum at 900 °C and CH_4 yield fluctuates in a certain range. V_g and G_v gradually increase from 0.137, 0.311 Nm^3/kg to 0.256, 0.425 Nm^3/kg, respectively. When 850DS8/DS is 1, Y_i gradually increases. η_C increases from 64.71% to 89.93%. V_g and G_v increase from 0.138, 0.289 Nm^3/kg to 0.267, 0.454 Nm^3/kg, respectively.

High temperature is conducive to the decomposition of DS and the secondary cracking of tar (tar → H_2 + CO + C_nH_m), resulting in more volatiles. Therefore, η_C, V_g and G_v both show apparent uptrend. Furthermore, as temperature rises, the gasification of carbon (C + H_2O → H_2 + CO, C + CO_2 → 2CO) which is an endothermic reaction will be promoted. While the reaction between CO, H_2 with OC to produce CO_2, H_2O which is an exothermic reaction will be inhibited. Thus, more CO,

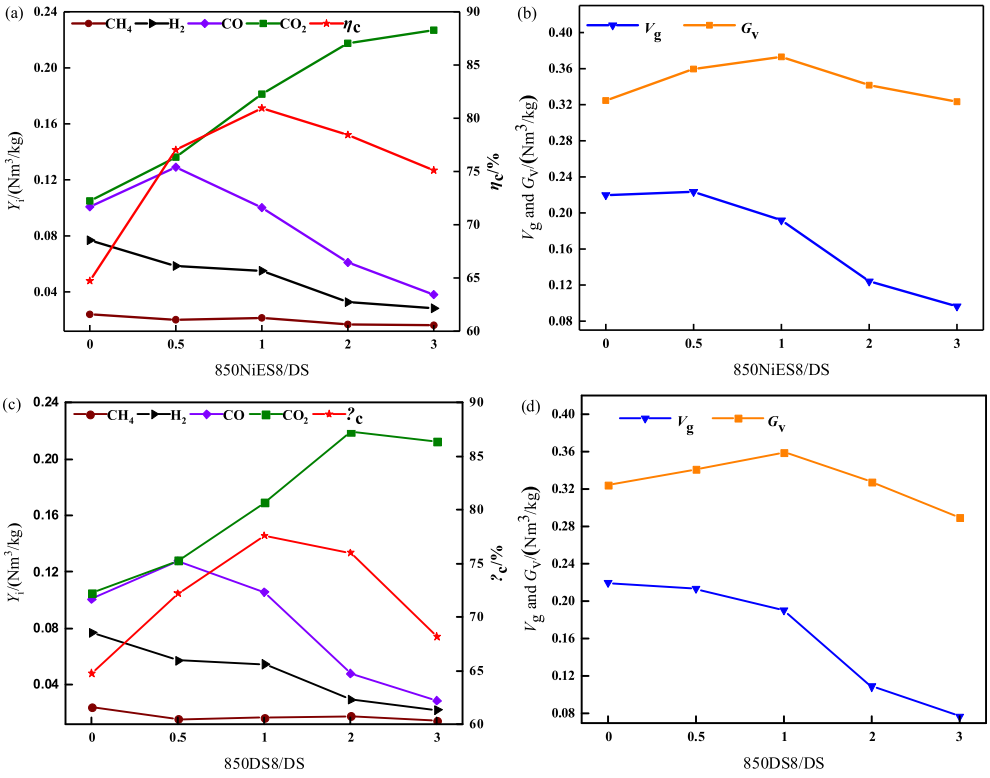

Fig. 2. Effect of 850NiES8/DS and 850DS8/DS on DS gasification at 850 °C (gas sampling time: 40 min).

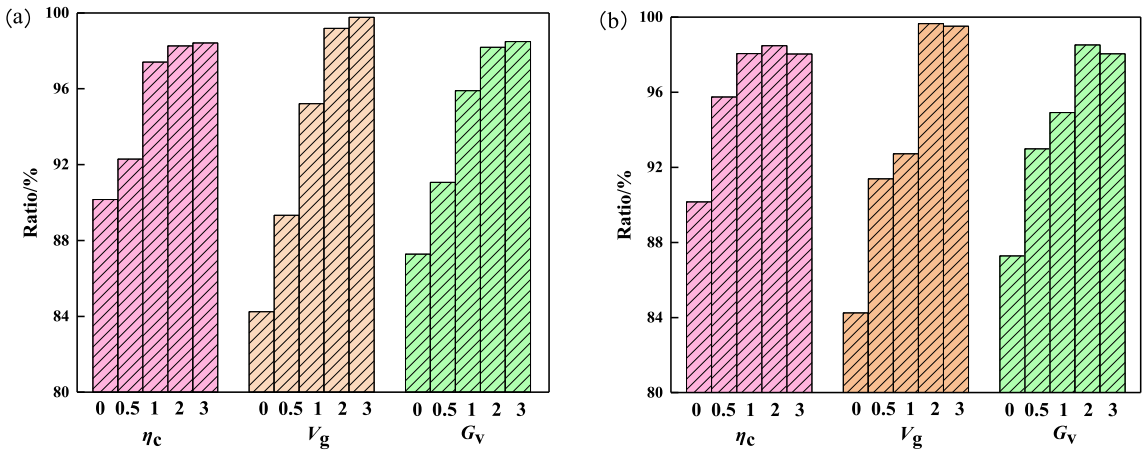

Fig. 3. Effect of (a) 850NiES8/DS and (b) 850DS8/DS on the ratios of DS gasification η_C, V_g, and G_v to the results of 40 min gas sampling time (gas sampling time:20 min).

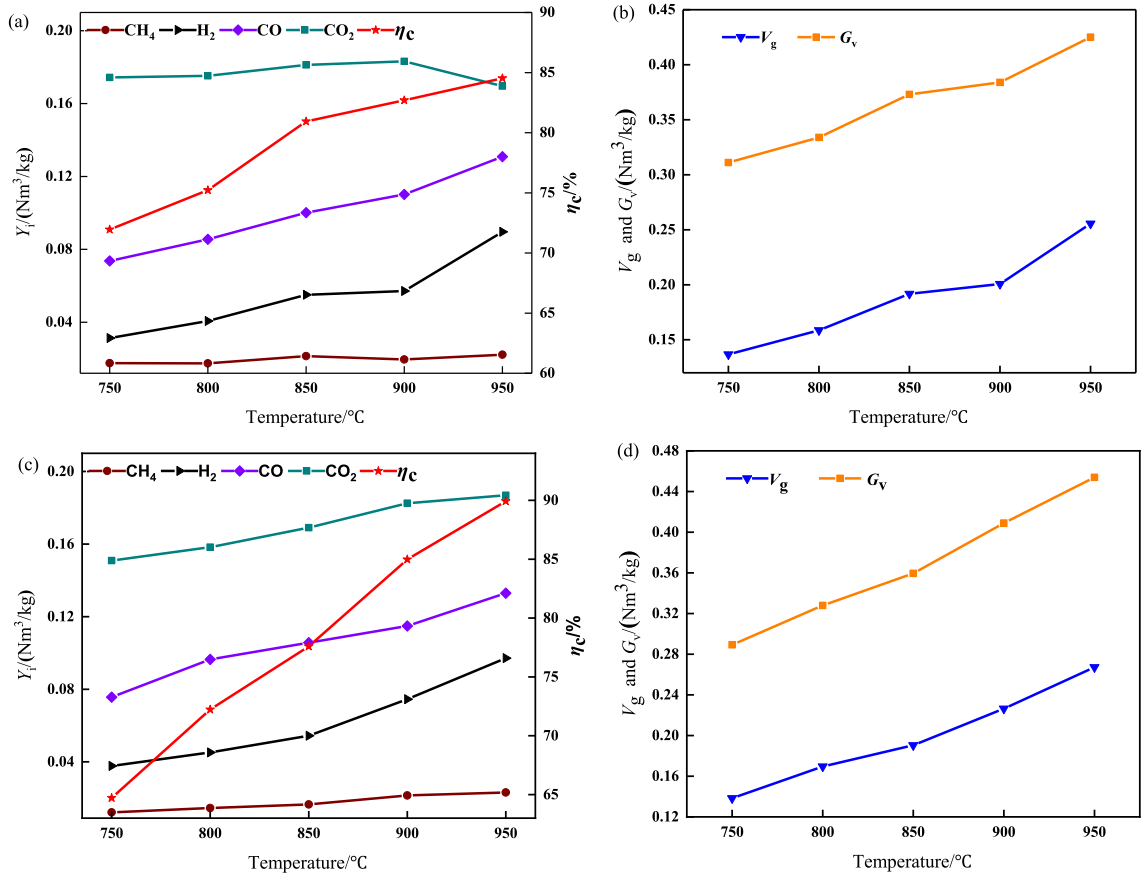

Fig. 4. Effect of reaction temperature on DS gasification (gas sampling time: 40 min): (a-b) at 850NiES8/DS of 1, (c-d) at 850DS8/DS of 1.

H_2, CH_4 are produced, the consumption of CO, H_2 and the production of CO_2 will be reduced. The reforming reaction of methane ($CH_4 + H_2O \rightarrow 3H_2 + CO$) is an endothermic reaction which contributes to the downtrend of CH_4 yield as well as the uptrend of CO, H_2 yield.

It can be seen that 850DS8 is superior to 850NiES8 at 900 °C and 950 °C. Because Fe_2O_3 is more stable than NiO at high temperature. As shown in Fig. 5, the rise of reaction temperature accelerates the gasification of DS at 850DS8/DS of 1. However, the downtrend at 950 °C (at 850NiES8/DS of 1) may be because 850NiES8 sinters at high temperature.

4. Conclusion

Novel material of OCs was developed from NiES and DS. The composition, crystal and pore structure, reaction activity and redox behavior of OCs were investigated. The selected OCs were applied to DS CLG under different reaction conditions. Considering higher temperature, longer time, NiES and DS calcined at 850 °C for 8 h (850NiES8, 850DS8) were selected which are more conducive to achieve stable crystal structure and large specific surface area. 850NiES8 displayed better reactivity and redox behavior than that of 850DS8. The two OCs both promoted TG pyrolysis of DS, and more weight loss of DS was

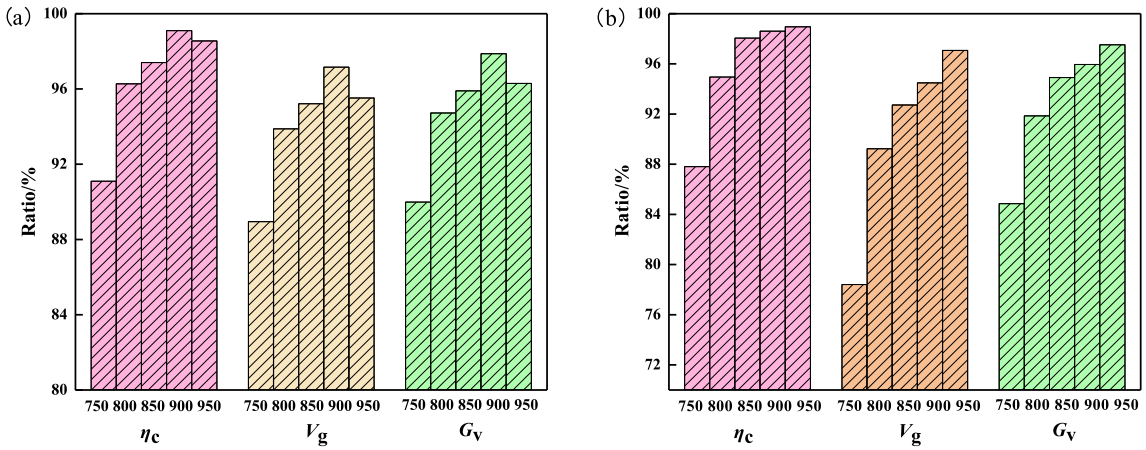

Fig. 5. Effect of reaction temperature on the ratios of DS gasification η_C, V_g, G_v to the results of 40-min gas sampling time (gas sampling time: 20 min): (a) at 850NiES8/DS of 1, (b) at 850DS8/DS of 1.

achieved by adding 850NiES8 when it was heated to 900 °C. The addition of 850NiES8, 850DS8 and higher reaction temperature significantly promoted DS CLG. 850NiES8 and 850DS8 increased η_C of DS to 80.94% and 77.59% respectively with acceptable energy recovery at 850 °C. V_g attained 0.223 Nm^3/kg when 850NiES8/DS was 0.5 at 850 °C, while η_C attained 89.93% when 850DS8/DS was 1 at 950 °C, which is better than previous studies. 850NiES8 and 850DS8 are two promising OCs, using which DS CLG provides new effective approaches for the resource utilization and harmless treatment of these two typical solid waste.

Declaration of Competing Interest

The authors declare that they have no known competing financial interests or personal relationships that could have appeared to influence the work reported in this paper.

Acknowledgement

This research was financially supported by State's Key Project of Research and Development Plan, China (2020YFC1908900), Key Special Project for Introduced Talents Team of Southern Marine Science and Engineering Guangdong Laboratory (Guangzhou), (GML2019ZD0101), Science and Technology Program of Guangdong Province, China (2021A1515012263 and 2019B110210003), and Science and Technology Program of Guangzhou, China (202002030365).

Appendix A. Supplementary material

Supplementary data to this article can be found online at https://doi.org/10.1016/j.wasman.2022.01.016.

References

Cao, Y., He, B., Yan, L., 2021. Cyclic reactivity of the sol–gel and graphite impregnation-derived Cu-based oxygen carriers for chemical looping with oxygen uncoupling. J. Therm. Anal. Calorim. 146 (4), 1833–1843. https://doi.org/10.1007/s10973-020-10163-6.

Chen, Q., Shen, L., Niu, X., 2016. Research on Chemical Looping Gasification of Sewage Sludge. J. Chinese Soc. Power. Eng. 36, 658–663.

Chen, X., Ma, R., Luo, J., Huang, W., Fang, L., Sun, S., Lin, J., 2021. Co-microwave pyrolysis of electroplating sludge and municipal sewage sludge to synergistically improve the immobilization of high-concentration heavy metals and an analysis of the mechanism. J. Hazard. Mater. 417, 126099. https://doi.org/10.1016/j.jhazmat.2021.126099.

Cheng, X., Gu, Z., Li, F., Zhu, X., Wei, Y., Zheng, M., Tian, D., Wang, H., Li, K., 2021. Enhanced resistance to carbon deposition in chemical-looping combustion of methane: Synergistic effect of different oxygen carriers via sequence filling. Chem. Eng. J. 421, 129776. https://doi.org/10.1016/j.cej.2021.129776.

Cuadrat, A., Abad, A., Adánez, J., de Diego, L.F., García-Labiano, F., Gayán, P., 2012. Behavior of ilmenite as oxygen carrier in chemical-looping combustion. Fuel Process. Technol. 94 (1), 101–112. https://doi.org/10.1016/j.fuproc.2011.10.020.

Deng, Z., Huang, Z., He, F., Zheng, A., Wei, G., Meng, J., Zhao, Z., Li, H., 2019. Evaluation of calcined copper slag as an oxygen carrier for chemical looping gasification of sewage sludge. Int. J. Hydrog. Energ. 44 (33), 17823–17834. https://doi.org/10.1016/j.ijhydene.2019.05.039.

Di, Z., Cao, Y., Yang, F., Cheng, F., Zhang, K., 2018. Studies on steel slag as an oxygen carrier for chemical looping combustion. Fuel 226, 618–626. https://doi.org/10.1016/j.fuel.2018.04.047.

Huang, Z., Zhang, Y., Fu, J., Yu, L., Chen, M., Liu, S., He, F., Chen, D., Wei, G., Zhao, K., Zheng, A., Zhao, Z., Li, H., 2016. Chemical looping gasification of biomass char using iron ore as an oxygen carrier. Int. J. Hydrog. Energy 41 (40), 17871–17883. https://doi.org/10.1016/j.ijhydene.2016.07.089.

Huang, Z., Deng, Z., Chen, D., Wei, G., He, F., Zhao, K., Zheng, A., Zhao, Z., Li, H., 2019. Exploration of Reaction Mechanisms on Hydrogen Production through Chemical Looping Steam Reforming Using $NiFe_2O_4$ Oxygen Carrier. Acs Sustain. Chem. Eng. 7 (13), 11621–11632. https://doi.org/10.1021/acssuschemeng.9b01557.

Ksepko, E., 2014. Sewage sludge ash as an alternative low-cost oxygen carrier for chemical looping combustion. J. Therm. Anal. Calorim. 116 (3), 1395–1407. https://doi.org/10.1007/s10973-013-3564-7.

Lin, Y., Liao, Y., Yu, Z., Fang, S., Lin, Y., Fan, Y., Peng, X., Ma, X., 2016. Co-pyrolysis kinetics of sewage sludge and oil shale thermal decomposition using TGA–FTIR analysis. Energy Convers. Manage. 118, 345–352. https://doi.org/10.1016/j.enconman.2016.04.004.

Liu, Q., Hu, C., Peng, B.o., Liu, C., Li, Z., Wu, K., Zhang, H., Xiao, R., 2019. High H_2/CO ratio syngas production from chemical looping co-gasification of biomass and polyethylene with CaO/Fe_2O_3 oxygen carrier. Energy Convers. Manage. 199, 111951. https://doi.org/10.1016/j.enconman.2019.111951.

Ma, Z., Zhang, S., Lu, Y., 2020. Activation Mechanism of Fe_2O_3-Al_2O_3 Oxygen Carrier in Chemical Looping Combustion. Energy Fuels 34 (12), 16350–16355. https://doi.org/10.1021/acs.energyfuels.0c02967.

Pérez-Astray, A., Adánez-Rubio, I., Mendiara, T., Izquierdo, M.T., Abad, A., Gayán, P., de Diego, L.F., García-Labiano, F., Adánez, J., 2019. Comparative study of fuel-N and tar evolution in chemical looping combustion of biomass under both iG-CLC and CLOU modes. Fuel 236, 598–607. https://doi.org/10.1016/j.fuel.2018.09.003.

Peng, G., Deng, S., Liu, F., Li, T., Yu, G., 2020a. Superhigh adsorption of nickel from electroplating wastewater by raw and calcined electroplating sludge waste. J. Clean. Prod. 246, 118948. https://doi.org/10.1016/j.jclepro.2019.118948.

Peng, G., Deng, S., Liu, F., Qi, C., Tao, L., Li, T., Yu, G., 2020b. Calcined electroplating sludge as a novel bifunctional material for removing Ni(II)-citrate in electroplating wastewater. J. Clean. Prod. 262, 121416. https://doi.org/10.1016/j.jclepro.2020.121416.

Sajjadi, B., Chen, W.-Y., Fan, M., Rony, A., Saxe, J., Leszczynski, J., Righetti, T.K., 2021. A techno-economic analysis of solar catalytic chemical looping biomass refinery for sustainable production of high purity hydrogen. Energ. Convers. Manage. 243, 114341. https://doi.org/10.1016/j.enconman.2021.114341.

Samprón, I., de Diego, L.F., García-Labiano, F., Izquierdo, M.T., Abad, A., Adánez, J., 2020. Biomass Chemical Looping Gasification of pine wood using a synthetic Fe_2O_3/Al_2O_3 oxygen carrier in a continuous unit. Bioresour. Technol. 316, 123908. https://doi.org/10.1016/j.biortech.2020.123908.

Sarafraz, M.M., Christo, F.C., 2020. Thermodynamic assessment and techno-economic analysis of a liquid indium-based chemical looping system for biomass gasification. Energy Convers. Manage. 225, 113428. https://doi.org/10.1016/j.enconman.2020.113428.

Silvester, L., Ipsakis, D., Antzara, A., Heracleous, E., Lemonidou, A.A., Bukur, D.B., 2016. Development of NiO-Based Oxygen Carrier Materials: Effect of Support on Redox Behavior and Carbon Deposition in Methane. Energy Fuels 30 (10), 8597–8612. https://doi.org/10.1021/acs.energyfuels.6b01520.

Tian, L., Chen, L., Gong, A.o., Wu, X., Cao, C., Liu, D., Chen, Z.-Q., Xu, Z.-F., Liu, Y., 2019. Separation and Extraction of Valuable Metals from Electroplating Sludge by Carbothermal Reduction and Low-Carbon Reduction Refining. Jom 72 (2), 782–789. https://doi.org/10.1007/s11837-019-03880-3.

Wang, C., Bi, H., Lin, Q., Jiang, X., Jiang, C., 2020a. Co-pyrolysis of sewage sludge and rice husk by TG–FTIR–MS: Pyrolysis behavior, kinetics, and condensable/non-condensable gases characteristics. Renew. Energy 160, 1048–1066. https://doi.org/10.1016/j.renene.2020.07.046.

Wang, K., Wang, F., Yu, Q., van Sint Annaland, M., Wang, Z., Xi, J., Zhang, Y., Xue, M., Du, S., 2021a. Understanding of the oxygen uncoupling characteristics of Cu Fe composite oxygen carriers for chemical-looping gasification. Fuel Process. Technol. 218, 106844. https://doi.org/10.1016/j.fuproc.2021.106844.

Wang, M., Gong, X., Wang, Z., 2018. Sustainable electrochemical recovery of high-purity Cu powders from multi-metal acid solution by a centrifuge electrode. J. Clean. Prod. 204, 41–49. https://doi.org/10.1016/j.jclepro.2018.09.020.

Wang, P., Pu, G., Liu, Q., Xiong, W., 2021b. Alkali metal modified iron-nickel oxygen carrier to produce hydrogen-rich synthesis gas by chemical looping gasification with pine sawdust. Int. J. Energ. Res. 45 (4), 5165–5176. https://doi.org/10.1002/er.6131.

Wang, X., Gong, Y., Wang, X., Jin, B., 2020c. Experimental and kinetics investigations of separated-gasification chemical looping combustion of char with an iron ore as the oxygen carrier. Fuel Process. Technol. 210, 106554. https://doi.org/10.1016/j.fuproc.2020.106554.

Wang, Y., Niu, P., Zhao, H., 2019. Chemical looping gasification of coal using calcium ferrites as oxygen carrier. Fuel Process. Technol. 192, 75–86. https://doi.org/10.1016/j.fuproc.2019.04.009.

Yang, J., Ma, L., Dong, S., Liu, H., Zhao, S., Cui, X., Zheng, D., Yang, J., 2017. Theoretical and experimental demonstration of lignite chemical looping gasification of phosphogypsum oxygen carrier for syngas generation. Fuel 194, 448–459. https://doi.org/10.1016/j.fuel.2016.12.077.

Yang, J., Ma, L., Yang, J., Guo, Z., Liu, H., Zhang, W., Wang, L., 2019a. Gasification Performance and Mechanism of High-Silicon Phosphogypsum Oxygen Carrier in Chemical Looping Gasification. Energ. Fuels 33 (11), 11768–11780. https://doi.org/10.1021/acs.energyfuels.9b02042.

Yang, J., Wei, Y.i., Yang, J., Xiang, H., Ma, L., Zhang, W., Wang, L., Peng, Y., Liu, H., 2019b. Syngas production by chemical looping gasification using Fe supported on phosphogypsum compound oxygen carrier. Energy 168, 126–135. https://doi.org/10.1016/j.energy.2018.11.106.

Yang, J., Liu, S., Ma, L., Liu, H., Yang, J., Guo, Z., Ao, R., Dai, Q., 2021. Syngas preparation by NiO–$CaSO_4$-based oxygen carrier from chemical looping gasification technology. J. Energ. Inst. 94, 191–198. https://doi.org/10.1016/j.joei.2020.09.003.

Zhang, L., Zhou, W., Liu, Y., Jia, H., Zhou, J., Wei, P., Zhou, H., 2020a. Bioleaching of dewatered electroplating sludge for the extraction of base metals using an adapted microbial consortium: Process optimization and kinetics. Hydrometallurgy 191, 105227. https://doi.org/10.1016/j.hydromet.2019.105227.

Zhang, R., Zhang, J., Guo, W., Wu, Z., Wang, Z., Yang, B., 2021a. Effect of torrefaction pretreatment on biomass chemical looping gasification (BCLG) characteristics: Gaseous products distribution and kinetic analysis. Energ. Convers. Manage. 237, 114100. https://doi.org/10.1016/j.enconman.2021.114100.

Zhang, S., Gu, H., Zhao, J., Shen, L., Wang, L., 2019. Development of iron ore oxygen carrier modified with biomass ash for chemical looping combustion. Energy 186, 115893. https://doi.org/10.1016/j.energy.2019.115893.

Zhang, S., Feng, Y., Guo, X., 2021. Redox Performance of Cu-Doped Fe_2O_3/Al_2O_3 as Oxygen Carriers for Chemical Looping Hydrogen Production. Energ. Fuels 35 (1), 626–635. https://doi.org/10.1021/acs.energyfuels.0c03496.

Zheng, A., Fan, Y., Wei, G., Zhao, K., Huang, Z., Zhao, Z., Li, H., 2020. Chemical Looping Gasification of Torrefied Biomass Using $NiFe_2O_4$ as an Oxygen Carrier for Syngas Production and Tar Removal. Energy Fuels 34 (5), 6008–6019. https://doi.org/10.1021/acs.energyfuels.0c00584.

Zhou, W., Zhang, L., Peng, J., Ge, Y., Tian, Z., Sun, J., Cheng, H., Zhou, H., 2019. Cleaner utilization of electroplating sludge by bioleaching with a moderately thermophilic consortium: A pilot study. Chemosphere 232, 345–355. https://doi.org/10.1016/j.chemosphere.2019.05.185.